IOP Conf. Series: Materials Science and Engineering **449** (2018) 012025 doi:10.1088/1757-899X/449/1/012025

Prevention of Hazardous Failure of the Turbine Rotor Due to Its Overspeed

Y.A. Nozhnitsky[1] and A.N. Servetnik[1]

[1]Central Institute of Aviation Motors (CIAM), 2, Aviamotornaya st., Moscow 111116, Russia

nozhnitsky@ciam.ru

Abstract. Causes of defects that can lead to the turbine rotor overspeed and subsequent hazardous consequences are considered. Methods of preventing unacceptable overspeed and confirmation of the sufficient strength of the turbine rotor are analyzed. Particular attention is paid to the developed method of calculating burst speed of the rotor. A comparison of the numerical and experimental data on basis of relation between radial displacements during spin tests, burst speed, high-speed image acquisition, fracture origin and fracture confirms possibility to use the developed method of calculations. The presented method allows to adjust the value of a disc rotation rate during certification spin tests to ensure that a disc with the worst mechanical properties will not burst in operation and to take into account differences in the design and loading conditions between the disc for spin tests and disc for operation.
If the identification of model's material parameters was performed based on disc's tensile tests and spin tests, then for a disc of another design from the same material only calculations can be used.

1. Introduction.

Fracture of the turbine rotor during overspeed is one of the most potentially hazardous defects of a gas turbine engine (GTE). Only in rare cases (for some auxiliary engines) it is possible to reliably exclude hazardous consequences (in particular, escape of fragments with high kinetic energy through the engine cases; uncontrolled fire; failure of engine mounts, leading to separation of the engine from the aircraft) when the turbomachine rotor (disc, blisk, bling, drum, centrifugal wheel, hereinafter referred to as a disc) fails.

This article examines some issues related to providing and confirming load-carrying capacity of a disc, taking into account possible overspeed. Turbomachine disc must have sufficient strength to withstand both normal operation conditions and conditions when maximum permissible operating speed is exceeded, including conditions after failure of the most critical component with respect to rotor overspeed or system or a combination of this failure with any failure of a component or system, which cannot be detected during a routine preflight check or during normal flight operation. It should be confirmed that even a disc made of a material with the combination of most adverse material properties and dimensional tolerances has sufficient strength [1-3].

2. Causes of a turbine rotor overspeed and measures to prevent unacceptable overspeed.

The turbomachine disc can experience overspeed, for example, due to a defect in engine control system, which results in an increased amount of fuel being supplied to combustion chamber; due to

failure of a reduction gear connecting turbine rotor and power consumer; failure of fan's (compressor's) impeller, etc. However, in practice, the most difficult task is to confirm sufficient strength of the turbine disc after breaking kinematic connection with a power consumer as a result of failure, displacement or disconnection of shafts. In this case, the overspeed of the turbine disc before its failure can occur in a fraction of a second and reaction speed of a pilot does not allow to take any action in such a short time. At the same time, when the disc is fractured under the conditions of overspeed, the kinetic energy of the fragments is especially high. Therefore, in accordance with requirements of airworthiness standards [1-3], fracture, disconnection or displacement of shafts should not lead to hazardous failure [4-6]. Experience shows that failure of a shaft system can occur due to various reasons – failure of rotor's coupling parts, shaft's manufacturing flaws (including material defects); corrosion of the shaft's material (including stress corrosion); overheating of the shaft's material due to fire (for example, when fuel mixes with oil in a fuel-oil heat exchanger), due to a breakthrough of hot gas into the shaft cavity, due to loss of spline coupling lubrication, due to the shaft contact with adjacent parts (including, for example, a result of flexural deformations, a significant imbalance of the rotor after blade-off, a failure of a bearing or other part adjacent to the shaft), including event, when load reduction device has been activated to reduce the load after blade-off conditions; fatigue (as a result, for example, of flexural or torsional oscillations, particularly, when pressure in the fuel system of the engine fluctuates), etc.

Fracture of a high-pressure turbine (HPT) shaft usually immediately leads to surging; so HPT rotor overspeed due to the shaft failure is limited. Nevertheless, the absence of a hazardous failure should be confirmed in the case of HPT shaft failure. More dangerous are shaft failures in intermediate-pressure turbines (in three-shaft engines), low pressure turbines (LPT), free power turbines, and turbounits (turbostarters, turbo-generators, turbo-refrigerating units).

To prevent a hazardous effect due to shaft fracture, a set of measures is usually used, including prevention of a defect, which can lead to shaft failure; employment of diagnostic methods of engine technical condition, which allow identifying such defects at an early stage of their development; decrease in criticality of defect development. For example, to prevent failure of LPT shaft, a large set of measures is used, selected on the basis of FMECA analysis including provision of high quality shaft manufacturing (like for the main engine parts); substantiated choice of coatings and lubricants for shafts and adjacent parts (taking into account possible corrosion); provision of sufficient shaft strength under operating conditions, including confirmation of the shaft's durability taking into account possible defects and, possibly, limitation of the designated service life; elimination of the possibility of hazardous overheating of a shaft material due to friction of the shaft with other parts by installation of a bumper between high and low pressure rotor shafts, application of heat-resistant coating of LPT shaft; installation of a bearing on an intermediate part, and not directly on the shaft; selection of pressure distribution, which excludes possibility of hot gas breakthrough into the shaft cavity; elimination of the possibility of fuel and oil mixing; application of rotor vibration dampers; etc.

Experience shows that probability of turbomachine shaft failures exceeds extremely low probability, and causes of the shaft failures are very numerous. Therefore, the design of the engine should ensure that turbine rotor overspeed is limited, and that sufficient load-carrying capacity of the rotor, taking into account possible overspeed, must be reliably confirmed.

Design solutions that limit a turbine engine's rotor overspeed in an event of shaft failure, are shown in Table 1.

Table 1. Design solutions that limit turbine rotor overspeed in an event of a shaft failure

Solution	Advantages	Disadvantages and issues

Ranking of integrity in a "blade airfoil – blade root – disc" system, which ensures the initial fracture of the blades in their root section during rotor overspeed	Effective regardless of at which section shaft was fractured (to the left or to the right of a thrust bearing)	It is necessary to prevent escaping through engine case fragments, formed during fracture of multiple blades at overspeed conditions
		High cost of subsequent engine repairs
Fitting a rotor turbine onto stator after axial downstream displacement of the rotor as a result of shaft failure (for example, using banana-shaped nozzle blades to arrange guaranteed connection of nozzle vanes and rotor blades and subsequent (mass fracture "meshing") of the blades)	Relative simplicity	Effective only when shaft is fractured at the right side of thrust bearing
		Time required for rotor displacement in axial direction to contact a stator should be much less than time to rotor fracture due to overspeed (a fraction of a second).
		Guaranteed fitting of the rotor on the stator is necessary, which eliminates formation of a sliding bearing and provides dissipation of the rotor energy due to friction between rotor and stator, as well as fracture of blades and vanes
		Difficulty of determining possible rotation rate during overspeed (without special test)
		High cost of subsequent engine repair
Cutting turbine rotor blades at rotor displacement after shaft failure (usually used in single-stage turbines)	Relative simplicity	The same as with axial displacement of a rotor with meshing of rotor blades and nozzle vanes
		Possibility of nonlocalized rotor fragments escaping case (for example, outside of turbo-starter's radial armor protection)
Mechanical system for fuel cut-off after shaft failure	Possibility of ensuring required speed	Impossibility of monitoring system's workability at service conditions
	Relatively good condition of the engine after an event	
Electronic system for abrupt increase of fuel supply for instantaneous surging after shaft failure	Relatively good condition of the engine after an event	Effective only in some cases (to prevent the intermediate-pressure turbine rotor overspeed)

	Possibility of monitoring system's workability at service conditions	It is needed to test the electronic system's performance under external influences (EMC, etc.)
		It is needed to prevent the engine shut down on a false signal
Electronic system for fuel cut-off after shaft failure	Relatively good condition of the engine after an event	Reliability and efficiency depend on the choice of type, number, layout of sensors, choice of structure (number of channels) and algorithm of the system
	Possibility of monitoring system's workability at service conditions	It is needed to test the electronic system's performance under external influences (EMC, etc.)
		Difficulty of determining possible rotation rate during overspeed
		Required limit of a rotor's rotation rate (speed) is not always ensured

When using a system based on the meshing of rotor and stator blades of an engine turbine in an event of axial displacement of the turbine rotor after the shaft fracture, it should be shown that the shaft fracture to the left of the thrust bearing (in which case the rotor is not displaced in the axial direction) is an extremely unlikely event. In this case, all possible causes of shaft failure should be considered. Additionally, it is important that, in an event of axial displacement of the turbine rotor, contact between engine's rotor and stator occurs at airfoils, otherwise a sliding bearing may form and rotor's overspeed will continue.

The electronic system is usually realized as a separate unit from the main control system and is provided with the power supply capability from the backup source. To increase reliability of the engine's turbine's electronic overspeed protection system, a two-channel system with two sensors in each channel is used. The choice of sensors' location is also important for ensuring their high reliability. Two-channel solution allows the engine to continue to operate when one of the system's channels fails, which is important for ensuring reliability centered maintenance (RCM).

Sometimes protection against unacceptable overspeed of an engine's turbine disc should be carried out by combined use of various solutions – for example, by combined use of an electronic fuel cut-off system, and in conditions where the speed of this system may not be sufficient – a system based on integrity ranking of elements in the "blade-disc" system.

In some cases, to confirm the absence of a hazardous failure in an event of engine's shaft fracture, it is necessary to carry out specific expensive engine test with shaft cutting. However, more often confirmation of the sufficient strength of a turbine disc under conditions of its possible overspeed is carried out on the basis of a spin testing of the disc and (or) a calculation of disc burst speed.

An estimation of possible rotation rate of a disc during overspeed is an independent task, which is not considered here. The method for calculating burst disc speed is considered below.

3. Numerical simulation of a disc burst speed

3.1. Description of a model

The finite element method (FEM) is the most effective tool for calculating the stress-strain state of a disc under conditions of overspeed. In papers [7-8], possibilities of using FEM for the calculation of plastic deformations in turbine discs GTE using the theory of plasticity are shown and a satisfactory

conformity between calculated and experimental values of a disc's burst speed is obtained (the difference was not more than 6%).

The basis of the calculation method is a step-by-step calculation of a disc using FEM with an increase of the rotation rate. We consider active (unidirectional) loading, in which hardening of the material is isotropic. We consider loading of the disc as a quasi-static process. Such assumptions are advantageous for reducing the time of the iterative solution. In this case, the parameter characterizing hardening of the material must be obtained at a deformation rate corresponding to the deformation rate of the disc during overspeed.

The process of transition of a disc from an elastic to an elastoplastic state performs step-by-step. First, the most stressed local zones (holes, fillets, slots, etc.) undergo plastic deformation, and then the plastic deformation extends further into the hub and web of the disc. Considering that the time it takes the disc to overspeed under operating conditions is a fraction of a second, we assume isothermal deformation process of the disc, i.e. neglected both by the internal release of heat due to plastic deformation, and by heating of the disc from external sources.

Taking into account the type of the disc's loading, we use isothermal theory of plasticity with isotropic hardening. Total deformation increments are split into elastic $\{\Delta\varepsilon^{el}\}$ and plastic deformation $\{\Delta\varepsilon^{pl}\}$:

$$\{\Delta\varepsilon\} = \{\Delta\varepsilon^{el}\} + \{\Delta\varepsilon^{pl}\}. \quad (1)$$

The increments of the elastic strain components are related to the increments of the stress components $\{\Delta\sigma\}$ by Hooke's law through the matrix of elastic moduli [D]:

$$\{\Delta\varepsilon^{el}\} = [D]^{-1}\{\Delta\sigma\}. \quad (2)$$

Plastic deformations are determined by introducing three characteristics of the material's nonlinear behavior: the yield function f, which characterizes conditions of plastic flow during complex stress state, the flow rule determining the direction of development of plastic deformation, and the hardening function $\overline{\sigma}$, which determines how f varies during plastic flow.

During plastic flow stresses must be on the loading surface, i.e. two conditions must be fulfilled simultaneously:

$$f(\{\sigma\}, \overline{\sigma}) = 0, \quad (3)$$

$$df = 0. \quad (4)$$

Increments of the plastic deformation components with the use of associative plasticity are connected through the derivatives of the yield function f with respect to the corresponding stress components:

$$\{\Delta\varepsilon^{pl}\} = \lambda\left\{\frac{\partial f}{\partial\sigma}\right\}, \quad (5)$$

Where

λ – non-negative parameter that determines the value of the increment of the plastic flow.

In the practice of disc numerical simulation, the yield function with a Mises yield condition is widespread:

$$f = \left(\frac{1}{2}[(\sigma_1 - \sigma_2)^2 + (\sigma_2 - \sigma_3)^2 + (\sigma_3 - \sigma_1)^2]\right)^{1/2} - \overline{\sigma}(\bar{\varepsilon}^{pl}, T). \quad (6)$$

Where

$\sigma_1,\ \sigma_2,\ \sigma_3$ – principal stresses;

$\overline{\sigma}(\bar{\varepsilon}^{pl}, T)$ – function of material hardening, which depends on the accumulated plastic deformation $\bar{\varepsilon}^{pl}$ and temperature T.

Assuming that this function is independent of the type of stress state, we use tensile curves at different temperatures. Usually $\overline{\sigma}(\bar{\varepsilon}^{pl}, T)$ is given in the form of piecewise linear functions, and the intermediate values are determined by linear interpolation.

The justification for using (6) is the multiple validations performed for various classes of metallic materials. However, calibration of this model during the spin rig testing of an aircraft's GTE turbine disc made from Udimet 720 at normal temperature [9] have shown that the best correspondence of the

numerical and experimental data is achieved when using Tresca yield condition, which can be represented in yield function as:

$$f = \frac{1}{2}[(\sigma_1 - \sigma_2) + (\sigma_2 - \sigma_3) + (\sigma_3 - \sigma_1)] - \bar{\sigma}(\bar{\varepsilon}^{pl}, T). \quad (7)$$

To study the influence of the yield condition on the burst speed, we used the non-quadratic yield function with Hosford yield condition [10]:

$$f = \left(\frac{1}{2}[(\sigma_1 - \sigma_2)^a + (\sigma_2 - \sigma_3)^a + (\sigma_3 - \sigma_1)^a]\right)^{1/a} - \bar{\sigma}(\bar{\varepsilon}^{pl}, T). \quad (8)$$

Where

a – parameter.

Tresca (a=1) and Mises (a=2 or a=4) yield conditions are special and limiting cases of the Hosford yield condition [10]. For a> 4, the yield condition lies between the limit curves and tends to Tresca yield condition for $a \to \infty$.

Calculation of plastic deformations within each iteration is performed using the return mapping algorithm [11]. The main problem of calculating plastic deformations under overspeed conditions is a reliable determination of material model's parameters, including yield condition, hardening function and failure criterion. These model's parameters can be identified from tensile testing of smooth specimens and spin testing of a model disc of the same material [12-13]. For the purpose of experimental adjustment of the method, two identical workpieces of a disc made of heat-resistant steel were manufactured. The disc for burst spin test was made from the first workpiece, and from the second - ten cylindrical specimens with a diameter d_0=6 мм, cut from different areas of the disc.

3.2. Identification of material model parameters

3.2.1. Identification from tensile test. The tensile test was carried out in accordance with ASTM E8M Standard at normal temperature at a rate of 0.3 mm/min with the installation of an extensometer on the body of the specimen.

Based on mean values of mechanical properties, the tensile curve is shown in Figure 1a (the dashed line shows the area after the beginning of the necking, which is not used in calculations). True stress vs. true plastic strain diagram (Figure 1b) was determined assuming a constant volume of material before and after plastic deformation, based on the following relations:

$$\sigma_{true} = \sigma(1 + \varepsilon), \quad (9)$$

$$\varepsilon^{pl}_{true} = \ln(1 + \varepsilon) - \sigma_{true}/E. \quad (10)$$

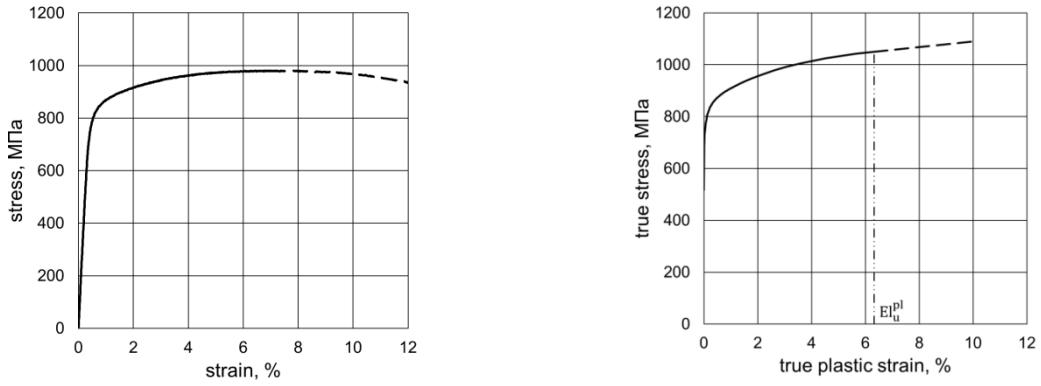

a) b)

Figure 1. Average tensile curve (a) and true stress vs. true plastic strain diagram (b)

We used true stress vs. true plastic strain diagram in the calculations as a hardening function $\bar{\sigma}(\bar{\varepsilon}^{pl}) = \sigma_{true}(\varepsilon^{pl}_{true})$. The dashed l function to ensure the convergence of the solution. Uniform

plastic elongation El_u^{pl} (as a part of uniform elongation) was considered a critical strain, after which burst of the disc begins.ine in Figure 1b shows a linear extrapolation of the hardening

3.2.2. *Identification from burst spin test.* We carried out the burst spin test of the disc (Figure 2) at normal temperature with increasing rotation rate linearly [14]. Loading rates of the disc and samples were approximately equal. During the test, we recorded the rotation rate and elongation of the outer diameter of the disc by two linear eddy-current sensors (using two sensors located at diametrically opposite points).

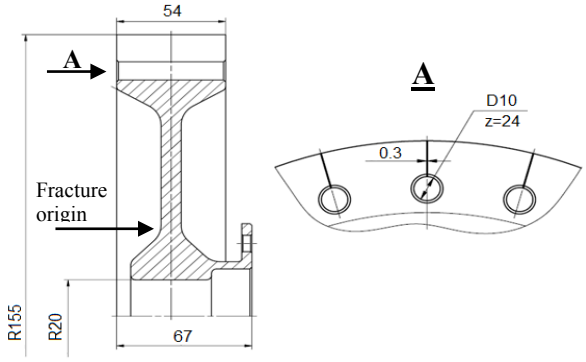

Figure 2. Drawing of the model disc (dimensions are in mm, z - number of orifices)

Disk burst at a rotation rate ω^{EXP} = 24282 rpm, while the radial displacement of the outer diameter of the disc at the time of burst was u^{EXP}=2.2 mm. Photography of disc after disk is shown in Figure 3. Fracture origin of the disc occurred along a cylindrical cross-section with the formation of a necking. Fracture of the disc along the meridian cross-sections passing through the holes is secondary.

We performed simulation of the disc overspeed via MSC. Marc on the disc sector with an angle α=15 ° (α=360/z). During formation of the finite element mesh, we took into account real geometric dimensions of the disc after manufacturing, determined by the results of 3D scanning. We divided the disk sector by first order hexahedral finite elements. On the boundaries of the sector, we set circumferential displacements to zero. Also, we fixed the model in one node in the axial direction to prevent it from moving as a rigid body. The values of the density and the Poisson's ratio are taken from the reference data.

The increase in the rotation rate was carried out with an even step: the first step corresponded to a rotation rate of 15,000 rpm; at the next steps rotation rate increased by 300 rpm.

A comparison of the results of the disc radial displacement calculations along the outer diameter under the condition of the Mises yield condition and the close to the Tresca yield condition (a=2 and a=100 in Eq. (8)), with experimental data is shown in Figure 4. In a range of rotation rates from 0 to 18000 rpm, the disc is deformed elastically, and correlations between calculated/experimental displacements of the disc coincide in this range. After reaching rotation rate of 18000 rpm, a deviation of the radial displacements from the elastic line is observed, which indicates elastoplastic deformation of the disc. Numerical displacements obtained with Mises yield condition and experimental displacements have a similar pattern over the entire range of rotation frequencies. For this material, Mises yield condition ensures better conformity of calculated and experimental data on radial displacements than Tresca yield condition. In this case, the accepted hypotheses about isotropic hardening and the associated plasticity can be considered acceptable.

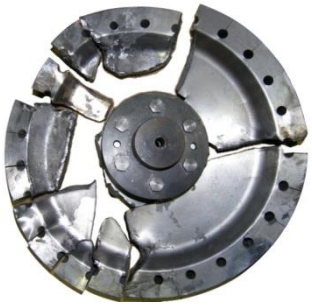

Figure 3. Photography of disc after burst

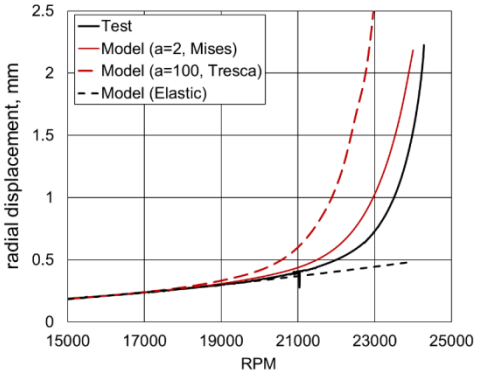

Figure 4. Experimental and numerical (a=2 and a=100) results of disc radial displacement

Distributions of the plastic strain intensity ε_i^{pl} of the disc at rotational rates of 23400, 23700 and 24000 rpm are shown in Figure 5. Plastic deformation reaches a maximum value in the disc web in the area, which corresponds to the fracture origin. At a rotation rate of 23400 rpm, the value of plastic deformation was 6.0% (see Figure 5a) and almost reached a critical strain El_u^{pl}= 6.3 %. Given the presence of a necking in the disc after the tests, we can assume that the fracture of the disc occurred with higher El_u^{pl}. At a rate of 24000 rpm (see Figure 5c), plastic deformations are already distributed over the entire section A-A.

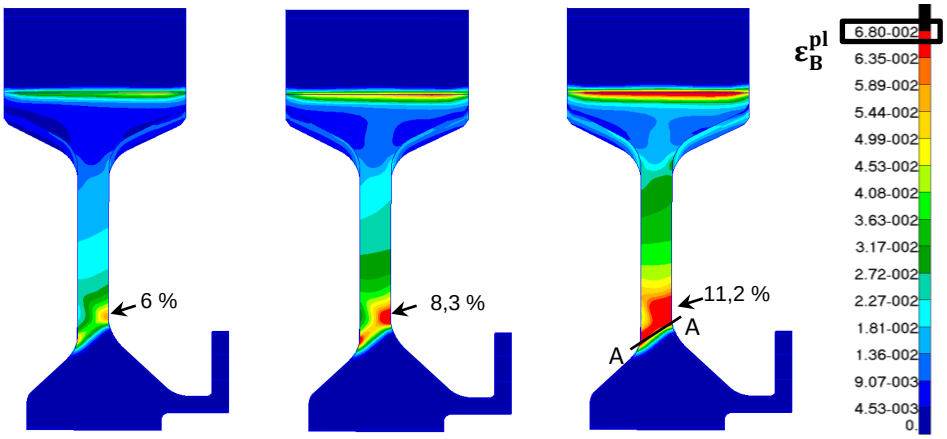

a) 23400 rpm b) 23700 rpm c) 24000 rpm

Figure 5. Distribution of the plastic strain intensity in a disc at different rotation rates

If we take into account that at the last loading step the calculated value of the radial displacement of the disc (u_r=2,18mm at 24000 rpm) is close to the experimentally determined value of the radial displacement of the disc at the moment of burst (u^{EXP}=2,2 mm at ω^{EXP} = 24282 rpm, see Figure 4), then the limiting state at which the disc burst, can be considered an attainment of plastic strain intensity equal to critical strain in an entire unsafe cross-section:

$$\varepsilon_{i,\ \text{cross-section A-A}}^{pl} = El_u^{pl}. \qquad (11)$$

3.2.3. Discussion on the results

According to (11), the burst speed of the disc is $\omega^{NUM(1)}$ = 24000 rpm, and the difference between numerical and experimental burst speed − $\Delta^{(1)}$=1 %. The fracture criterion (11) is not local. An

additional justification for this fact is the detection of a necking at a radius R=55 mm after burst of the disc.

The smooth specimen necking is determined by the reduction of diameter:

$$\psi_d = \frac{d_0 - d_k}{d_0} = 1 - \sqrt{1 - \psi}, \quad (12)$$

Where

d_k – diameter of the specimen in the neck area after burst;

ψ – reduction of area.

The web disk necking is determined by the reduction of web:

$$\psi_h = \frac{H_0 - H_k}{H_0} \quad (13)$$

The average value of reduction of diameter is ψ_d=0.26, and reduction of web − ψ_h=0.21. Thus, the change in the dimensions of the specimen and the disc in the plastic deformation localization zone turned out to be sufficiently close to each other.

In practice, local fracture criteria are used to calculate burst speed, which are presented in papers [6-9, 15, 16]. For example, if as the fracture criterion we consider the equality of the maximum plastic deformation and critical strain:

$$\varepsilon^{\mathrm{pl}}_{\mathrm{i,\ max}} = \mathrm{El}^{\mathrm{pl}}_{\mathrm{u}}, \quad (14)$$

then the burst speed $\omega^{NUM(2)}$ = 23450 rpm and the difference between numerical and experimental burst speed − $\Delta^{(2)}$=3.5 %.

To estimate the value of burst speed, it is often used average radial stress criterion [17]: a disc will burst when average radial nominal stress equals the tensile strength of the material. As well as for the average hoop stress criterion [18], one of the main drawbacks of the method is the lack of possibility to take into account the plastic characteristics of the material. According to this criterion $\omega^{NUM(3)}$=22400 rpm and $\Delta^{(3)}$=8 %.

Thus, to calculate the burst speed of a disc made from steel, it is preferable to use the fracture criterion (11), where plastic deformation is determined based on the isothermal theory of plasticity with the Mises yield condition and isotropic hardening. The advantage of the method is also detection of the fracture origin and the critical disk section.

Using the method described above, for a number of model disks and full-size discs of various designs made from steels, titanium and nickel alloys tested at normal and operating temperatures, we performed a comparison of the numerical and experimental data on basis of relation between radial displacements during spin tests, burst speed, high-speed image acquisition, fracture origin and fracture mode analysis. Based on the results of the research, we gave recommendations for disc burst speed analysis. It should be noted that for the disc made from nickel based superalloys Udimet 720 and EP741NP, for which fracture of the specimens in the tensile test occurs without necking, it has been shown that the use of the Tresca yield condition [3,10] and the local fracture criterion (14) is advantageous.

When calculating the load-carrying capacity of a disc, it is necessary to take into account the most unfavorable operating conditions of the engine during overspeed, the unfavorable combination of dimensional tolerances and the statistically minimum values of the material's mechanical characteristics [1-3]. The presented method also allows to adjust the value of a disc rotation rate during certification spin tests to ensure that a disc with the worst mechanical properties will not burst in operation and to take into account differences in the design and loading conditions between the disc for spin tests and disc for operation.

If the identification of model's material parameters was performed based on disc's tensile tests and spin tests, then for a disc of another design from the same material only calculations can be used.

Acknowledgments
All activities have been carried in CIAM. The authors are grateful for permission to publish the paper. The authors are grateful to the team led by M.E.Volkov for testing samples in CIAM laboratory.

References

[1] Aviation regulations. Part 33. Airworthiness of aircraft engines 2012 IAC
[2] 14 CRF, Part 33. Airworthiness Standards. Aircraft Engines 2014 FAA
[3] Certification Specifications for Engines (CS-E) 2015 EASA
[4] Engine and Turbosupercharger Rotor Overspeed Requirements of 14 CFR §33.27 2011 FAA, AC33.27-1A
[5] Turbine Overspeed Resulting from Shaft Failure 2012 EASA, Certification Memorandum EASA CM-PIFS-003 Issue 01
[6] Nozhnitsky Y A and Kuevda V K 2018 Prevention of a dangerous failure of a gas turbine engine due to fracture, disconnection or displacement of the shafts *Proc. of the Scientific and Technical Congress of Engine-building* Moscow 2 pp.267-276
[7] Servetnik A N 2012 Energy-based method for gas turbine engine disc burst speed calculation, *28th Congress of the International Council of the Aeronautical Sciences* ICAS 2012 Brisbane Australia 23-28 September 2012 pp.2443-2448
[8] Nozhnitsky Y A, Karimbaev K D and Servetnik A N 2012 Numerical simulation of spin testing for turbo machine discs using energy-based fracture criteria *Proc. ASME Turbo Expo*, Copenhagen, Denmark 11-15 June 2012 V.7 pp.35-40
[9] Maziere M, Besson J, Forest S, Tanguy B, Chalons H and Vogel F 2008 Overspeed burst of elastoviscoplastic rotating discs Part II: Burst of a superalloy turbine disc *European Journal of Mechanics A/Solids*, V.28 pp.428-432
[10] Hosford W 2005 Mechanical behavior of materials Cambridge University Press p.425
[11] Simo J C and T J R Hughes 1998 Computational Inelasticity Springer-Verlag New York, P.392
[12] Kuzmin E P and Servetnik A N 2014 Yield surface investigation of alloys during model disc spin tests *Science and Education: Scientific Publication* №5 pp.330-339
[13] Servetnik A N and Kuzmin E P 2014 Yield surface investigation of alloys during model disc spin tests *Proc. ASME Gas Turbine India Conf* GTINDIA2014 India Delhi 15-17 December 2014 p.3
[14] Nozhnitsky Y A, Fedina Y A, Shadrin D V, Servetnik A N, Baluev B A, Kanachkin A V, Lepeshkin A R, Tomashiov A A and Cherhyshev S A 2015 New possibilities of using spin rigs to provide gas turbine engine strength reliability *Vestnik of the Samara State Aerospace University* V.14 №3 part 1 pp.71-87
[15] Karimbaev K D and Servetnik A N 2008 Numerical modeling of turbo machine disc burst speed test *Herald of Aeroenginebuilding* №3 pp.130-134
[16] Servetnik A N 2012 Load-carrying capability simulation of aviation gas turbine engine disc *Handbook. An Engineering Journal* V.187 №10 pp.44-49
[17] Birger I A, Shorr B F, Dem'yanushko I V, Dulnev R A and Sizova R N 1975 Thermal strength of machine parts Mashinostroenie Moscow Russia p.454
[18] Stodola A 1927 Steam and Gas Turbine V.2 McGrow-Hill Book Co. Inc. New York N.Y. p.1080